NUCLEAR THEORY, Vol. 37 (2018)
eds. M. Gaidarov, N. Minkov, Heron Press, Sofia

From Nuclei to Neutron Stars with a Consistent Approach

F. Sammarruca, **Randy Millerson**

University of Idaho, 83844-0903 Moscow, Idaho, U.S.A.

Abstract. We discuss applications of nuclear and neutron matter equations of state based on high-quality chiral few-nucleon forces. First, we review an investigation of the relation between the neutron skin of a nucleus and the difference between the proton radii of the mirror pair with the same mass. Second, we address neutron star masses and radii obtained from equations of state based on most recent chiral nucleon-nucleon potentials up to fifth order of the chiral expansion together with the leading chiral three-nucleon force. We focus on the radius of a 1.4 $M_\odot$ neutron star, for which we predict values that are consistent with most recent constraints.

1 Introduction

Although finite nuclei are the natural arena to test nuclear forces in the many-body system, infinite matter is a suitable and convenient theoretical benchmark for in-medium nuclear forces. In particular, the equation of state (EoS) of neutron-rich matter, namely the energy per particle in isospin-asymmetric matter as a function of density, plays an outstanding role in remarkably diverse situations including: neutron drip lines, neutron skins, and the structure of neutron stars.

As we have done in all our recent endeavors, we apply high-quality few-nucleon interactions derived from chiral Effective Field Theory (EFT). Respecting the symmetry of (low-energy) QCD while employing degrees of freedom appropriate for low-energy nuclear physics (nucleons and pions), chiral EFT is a systematic approach to the development of nuclear forces which allows for a controlled expansion and a quantification of the uncertainty at each order of the perturbation theory. The reader is referred to, for instance, Ref. [1] for a comprehensive review.

In this paper, we concentrate on two of our most recent investigations. The first one concerns neutron and proton skins [2], for which we apply the EoS developed in Ref. [3]. In the second part of the paper, we move to considerations of neutron star radii [4]. For that purpose, we use the EoS developed in Ref. [5] which employ most recent and improved chiral potentials [6].

2 Proton Skins and Mirror Nuclei

Empirical information on neutron radii and neutron skins is limited and accompanied by considerable uncertainty (see, for instance, Ref. [7] and references therein for a summary of empirical constraints obtained from a variety of measurements [8–11]). Although future experiments [12] are planned which may be able to probe the weak charge density in ^{208}Pb and, possibly, in ^{48}Ca, other strategies to obtain related information are being investigated.

The possibility of extracting constraints on neutron skins from the knowledge of proton radii alone, specifically those of mirror pairs, is proposed in Ref. [13]. There, correlations between neutron skins and the slope of the symmetry energy are deduced using large sets of phenomenological interactions, specifically 48 Skyrme functionals. Furthermore, a correlation is found between the difference in the charge radii of mirror nuclei and the slope of the symmetry energy. The study presented in Ref. [14] is similar in spirit but is based on relativistic energy density functionals.

In Ref. [2], we have used microscopic EoS as opposed to phenomenological ones in order to explore the relation between the neutron skin of a nucleus and the difference between the proton radii of the mirror pair with the same mass. The EoS are obtained in Brueckner-Hartree-Fock calculations [3] employing high-quality nucleon-nucleon chiral potentials [1]. The microscopic equations of state are then used in the volume term of a liquid-drop energy functional. This makes the treatment of the volume term distinct from the one of a fully phenomenological study. The estimated theoretical errors include uncertainties due to variations of the cutoff in the range 450-500 MeV as well as an error (added in quadrature) to account for the uncertainty originating from the method we use to calculate the skins [7].

In the presence of perfect charge symmetry, the equality

$$R_n(Z,N) = R_p(N,Z) \tag{1}$$

must hold for mirror nuclei. Then, from the definition of the neutron skin,

$$S_n(Z,N) = R_n(Z,N) - R_p(Z,N)\ , \tag{2}$$

one can conclude, using Eq. (1), that

$$S_n(Z,N) = R_n(Z,N) - R_p(Z,N) = R_p(N,Z) - R_p(Z,N) \equiv \Delta R_p\ . \tag{3}$$

That is, the neutron skin of nucleus (Z,N) would be equal to the difference between the proton radii of the corresponding mirror pair. If charge radii could be measured accurately for mirror pairs in the desired mass range, then we could obtain the neutron skin of the (Z,N) nucleus from Eq. (3) after appropriate corrections are applied to account for charge effects.

In what follows, we pay particular attention to a specific range within medium mass nuclei, namely $A \approx 48 - 54$, see Table 1. This is an interesting and timely

Table 1. Proton skins, S_p, in the mass range 48-54.

Z	A	S_p (fm)	Z	A	S_p (fm)
20	48	-0.181 $\pm$ 0.010	24	52	-0.048 $\pm$ 0.007
28	48	0.316 $\pm$ 0.021	28	52	0.169 $\pm$ 0.013
22	50	-0.112 $\pm$ 0.010	26	54	0.008 $\pm$ 0.006
28	50	0.238 $\pm$ 0.016	28	54	0.112 $\pm$ 0.013

choice because of the vicinity to ^{48}Ca, whose neutron skin is likely to be the object of future experimental investigations together with ^{208}Pb based on parity-violating electron scattering.

In Table 2, 3, and 4, we address the relation between neutron skins and ΔR_p as defined in Eq. (3). Table 2 displays the neutron skin of the neutron-rich isotones from Table 1 in relation to ΔR_p, with and without Coulomb effects.

It is insightful to explore the relation between ΔR_p and $S_n(Z,N)$ for other chains. In particular, we investigate if and how such relation differs, quantitatively, among chains with different masses. For that purpose, we consider in Table 3 and 4 two *isotopic* chains, one of them in a mass range considerably different than the one studied in Table 2.

We observe that, for similar values of ΔR_p, the corresponding values of $S_n(Z,N)$ are approximately the same, regardless Z and N. Also, in all three cases the relation is approximately linear. It is important to stress that these relations are derived in a fundamentally distinct way as compared to those discussed in Ref. [13]. The latter are obtained varying the parameters of Skyrme models

Table 2. Relation between the neutron skin of nucleus (Z,N), $S_n(Z,N)$, and ΔR_p of the corresponding mirror pair for the isotone chain $N = 28$. The values in paranthesis are the results without Coulomb contribution (as a verification).

Z	N	$S_n(Z,N)$ (fm)	ΔR_p(fm)
20	28	0.181 $\pm$ 0.010 (0.229)	0.309 $\pm$ 0.023 (0.229)
22	28	0.112 $\pm$ 0.010 (0.162)	0.220 $\pm$ 0.019 (0.162)
24	28	0.048 $\pm$ 0.007 (0.103)	0.139 $\pm$ 0.016 (0.103)
26	28	-0.008 $\pm$ 0.006 (0.049)	0.066 $\pm$ 0.007 (0.049)

Table 3. Relation between the neutron skin of nucleus (Z,N), $S_n(Z,N)$, and ΔR_p for the isotope chain $Z = 20$.

Z	N	$S_n(Z,N)$(fm)	ΔR_p(fm)
20	22	0.015 $\pm$ 0.007	0.081 $\pm$ 0.008
20	24	0.073 $\pm$ 0.006	0.156 $\pm$ 0.014
20	26	0.128 $\pm$ 0.010	0.233 $\pm$ 0.019
20	28	0.181 $\pm$ 0.010	0.309 $\pm$ 0.023

Table 4. Relation between the neutron skin of nucleus (Z, N), $S_n(Z, N)$, and ΔR_p for the isotope chain Z=10.

Z	N	$S_n(Z, N)$ (fm)	ΔR_p(fm)
10	11	0.031 ± 0.005	0.071 ± 0.005
10	12	0.090 ± 0.005	0.140 ± 0.011
10	13	0.143 ± 0.010	0.204 ± 0.012
10	14	0.195 ± 0.010	0.269 ± 0.014

(each model constrained to produce a chosen value of the neutron skin in ^{208}Pb) for a fixed mirror pair. Here, the question being explored is to which extent these microscopic EoS might yield, within theoretical uncertainties, a unique relation between S_n and ΔR_p.

We find that the parameters of the predicted linear relation,

$$S_n = a(\Delta R_p) + b \,, \tag{4}$$

based upon the cases we have considered here, can be summarized as

$$a = 0.78 \pm 0.05 \,, \qquad b = -0.0385 \pm 0.0215 \,. \tag{5}$$

3 The Radius of a Typical Neutron Star

The EoS of neutron-rich matter is fundamentally important for systems ranging from the neutron skin (see previous section) to compact stars. In fact, the relation between the mass and the radius of neutron stars is uniquely determined by the EoS together with their self-gravity, making these compact systems remarkable testing grounds for both nuclear physics and general relativity. Following the recent detection by LIGO of gravitational waves from two neutron stars spiraling inward and merging, additional interest and excitement has developed around these most exotic systems. The LIGO/Virgo [15] detection of gravitational waves originating from the neutron star merger GW170817 has provided new and more stringent constraints on the maximum radius of a 1.4 $M_\odot$ neutron star, based on the tidal deformabilities of the colliding stars [16].

Here, we will briefly present and discuss some of our recent predictions of neutron star radii based on state-of-the-art nuclear forces [4]. The focal point is the radius of a star with mass equal to 1.4 $M_\odot$ (the typical mass of a neutron star), which we wish to predict with appropriate quantification of the uncertainty.

Chiral EFT is a low-energy theory and thus limitated in its domain of applicability. The chiral symmetry breaking scale, $\Lambda_\chi \approx 1$ GeV, limits the momentum or energy domains where pions and nucleons can be taken as suitable degrees of freedom. Moreover, the cutoff parameter Λ appearing in the regulator function suppresses high momentum components. Naturally, the amount of suppression depends on the strength of the cutoff, namely, the magnitude of the cutoff parameter Λ.

Central densities in neutron stars can be as high as several times the density of normal matter around saturation. As a consequence, the highest momenta in stellar matter fall outside the reach of chiral EFT. As a guidance for how to extrapolate chiral predictions to the high density domain, we note that, for a very large number of existing EoS, the pressure as a function of baryon density (or mass density) can be fitted by piecewise polytropes, namely functions of the form $P = \alpha\rho^{\Gamma}$ [17], where, in our notation, ρ denotes the baryon density.) We then extend the pressure predictions obtained from the chiral EoS using polytropes. We consider stellar matter with neutrons, protons, and leptons (electrons and muons) in β equilibrium, and determine the fractions of each species using conditions of β-stability and charge neutrality, see Ref. [4] for more details.

Next, we briefly describe the main features of the two-nucleon force (2NF) we have employed in our recent work. Those are described in details in Ref. [6].

The NN potentials from Ref. [6] are constructed at five orders of chiral EFT, from leading order (LO) to fifth order (N^{4}LO). Because the same power counting scheme and regularization procedures are applied across all orders, this set of interactions is more consistent than previous ones.

Furthermore, in these new potentials the long-range part of the interaction is fixed by the πN LECs as determined in the recent and very accurate analysis of Ref. [18]. As a consequence, errors in the πN LECs can essentially be ignored when addressing uncertainty quantification. Moreover, at the fifth order the NN data below pion production threshold are reproduced with the excellent χ^2/datum of 1.15.

Due to the complexity of the three-nucleon force (3NF) at orders higher than three, very often only the leading 3NF is retained. However, for the very important part of the 3NF which describes the two-pion exchange, complete calculations up to N^{4}LO are actually feasible. As shown in Ref. [19], the formal structure of the two-pion exchange 3NF is nearly the same at the third, fourth, and fifth orders. One can then add the three orders of 3NF contributions and parametrize them in terms of effective c_i LECs. This is the procedure we have adopted in constructing the EoS used in these present calculations, see Ref. [5] for a detailed description. In our Brueckner-Hartree-Fock calculations of nuclear and neutron matter, we use the non-perturbative particle-particle ladder approximation.

Note that no 3NF are present at leading and next-to-leading orders. Since NN data cannot be described at a satisfactory precision level below the third order, in what follows we will discuss predictions only at orders equal or above the third (N^{2}LO).

In Figure 1, we show the calculated total energy per particle in β-stable matter at the third, fourth, and fifth orders of the 2NF together with the leading 3NF.

To perform continuation of the microscopic EoS to high densities, we employ our microscopic predictions up to about $2\rho_0$. We then attach polytropes having different adiabatic indices, $P(\rho) = \alpha\rho^{\Gamma}$, imposing continuity of the

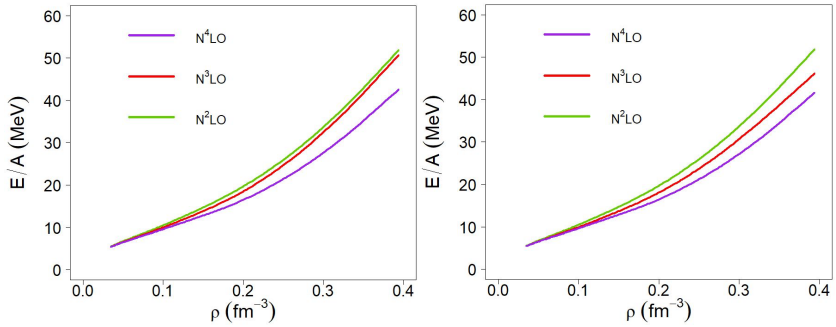

Figure 1. Energy per particle in β-stable matter as a function of density at the indicated orders for $\Lambda = 450$ MeV (left) and $\Lambda = 500$ MeV (right).

pressure. We vary the polytropic index between 1.5 and 4.5 (a range suggested by the literature [17]), and these extensions are calculated up to about $3\rho_0$. At this density, every polytrope is again joined continuosly with a set of polytropes spanning the same range. In this way, we include a large set of possibilities, with the EoS being "softer" or "stiffer" in one density region or the other, as it would be the case if phase transitions (most likely to non-hadronic degrees of freedom) were to take place.

This procedure, and the corresponding spreading of the pressure, is demonstrated in Figure 2. Note that only combinations of Γ_1 and Γ_2 which can support a maximum mass of at least 1.97 $M_\odot$, are retained, to be consistent with the observation of a pulsar with a mass of 2.01 ± 0.04 $M_\odot$ [20]. The mass and the radius as a function of the central density are shown in Figure 3 for those polytropic extensions consistent with a maximum mass of at least 1.97 $M_\odot$. The constraint of causality, requiring the speed of sound in stellar matter to be less than the speed of light, is also implemented.

We then proceed to estimate the value and the uncertainty for the radius of a 1.4 $M_\odot$ star, see Ref. [4] for more details. For the radius of the $1.4M_\odot$ star, we obtain

$$R^{N3LO} = (10.8 \ - \ 12.8) \text{ km} \, , \tag{6}$$

including truncation error, cutoff uncertainty, and of course the uncertainty originating from the polytropic extrapolation.

We find that the radius in this mass range is nearly insensitive to the extension at the larger densities, and shows only weak sensitivity to maximum variations of the first polytropic index. In other words, the uncertainty reported in Eq. (6) is relatively small given the huge uncertainty introduced in the pressure by the polytropic continuation. Note that the central densities we predict for the average-mass star are typically in the order of, and can exceed $3\rho_0$. These densities are at or above the one marked by the yellow line in Figure 2, where we see a very large spreding of the pressure. Clearly, this indicates that the ra-

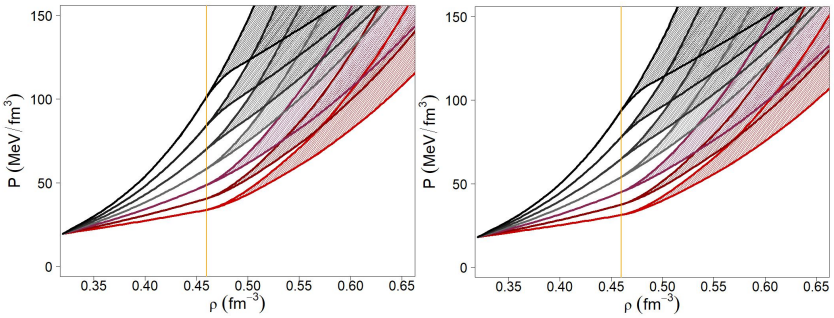

Figure 2. Spreading of the pressure at N^{3}LO from extension with polytropes as explained in the text. Left and right: $\Lambda = 450$ MeV and 500 MeV, respectively. The vertical coordinate axis and the vertical yellow line mark the two matching points where different EoS are joined. Only the combinations of polytropes which can support a maximum mass of at least 1.97 $M_\odot$ are retained.

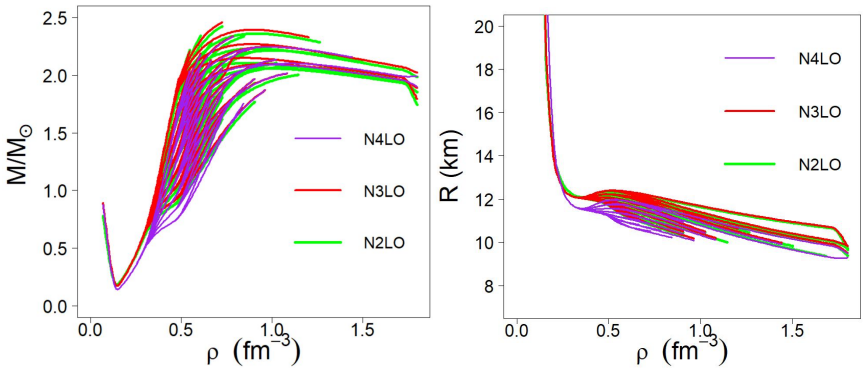

Figure 3. The neutron star mass (left) and the radius (right) *vs.* the central density at the indicated chiral order. The cutoff Λ is fixed at 450 MeV. The various curves are obtained with the polytropic extension as explained in the text. The purple curves are obtained extending the predictions at N^{4}LO, while the the red and the green curves are obtained extending the predictions at N^{3}LO and at N^{2}LO, respectively.

dius responds to pressures at much lower densities than those at the center of the star, consistent with earlier observations [21]. In summary, the radius of the average-mass star is largely determined by the microscopic theory and is nearly insensitive to the phenomenological continuations.

In Ref. [22], the authors determine the radius of a 1.4 M$_\odot$ neutron star to be between 10.4 and 12.9 km. Most recently, from LIGO/Virgo measurements the

radius of a 1.4 $M_\odot$ neutron star was determined to be between 11.1 and 13.4 km [15, 16]. Thus our chiral predictions are well within recent constraints.

4 Summary and Conclusions

We have summarized and discussed some of our recent results obtained from microscopic EoS based on high-quality chiral nuclear forces together with the leading chiral 3NF. As for the many-body method, we adopt the Brueckner-Hartree-Fock approach to infinite matter.

In one application, we explored neutron skins and proton skins of mirror nuclei. In another, we extended theoretical predictions of the EoS for beta-equilibrated matter past a few times normal density using a family of polytropic solutions. For the radius of a 1.4 $M_\odot$ neutron star, we explored the sensitivity of the predictions to the high-density extrapolation and confirmed that they depend only weakly on the high-density continuation method. Therefore, the predictions reflect the microscopic theory.

Work in progress and future plans include additional studies of the isovector properties of our most recent microscopic EoS, and further systematic applications in neutron-rich systems, both at zero and finite temperature.

With regard to improving consistency at the level of the chiral expansion, it must be noted that, although chiral EFT is presently the most fundamental and internally consistent approach to nuclear forces, its implementation in the many-body system presents serious challenges. Application of complete 3NF at 4th and 5th orders is a problem of enormous complexity, but necessary for a proper assessment of order-by-order convergence. At this time, we are encouraged that these new (softer) chiral interactions, particularly with a cutoff of 450 MeV, exhibit good perturbative behavior, as we have shown in Ref. [5], suggesting that they may be suitable for nuclear structure applications.

Acknowledgments

This work was supported by the U.S. Department of Energy, Office of Science, Office of Basic Energy Sciences, under Award Number DE-FG02-03ER41270.

References

[1] R. Machleidt and D.R. Entem, *Phys. Rep.* **503** (2011) 1.
[2] F. Sammarruca, *Front. Phys.* **6**:90 (2018).
[3] F. Sammarruca *et al.*, *Phys. Rev. C* **91** (2015) 054311.
[4] F. Sammarruca and Randy Millerson, arXiv: 1803.01437v2.
[5] F. Sammarruca, L.E. Marcucci, L. Coraggio, J.W. Holt, N. Itaco, and R. Machleidt, arXiv: 1807.06640.
[6] D.R. Entem, R. Machleidt, and Y. Nosyk, *Phys. Rev. C* **96** (2017) 024004.
[7] F. Sammarruca, *Phys. Rev. C* **94** (2016) 054317.
[8] M.B. Tsang *et al.*, *Phys. Rev. C* **86** (2012) 015803; and references therein.

[9] C. García-Recio, J. Nieves, E. Oset, *Nucl. Phys. A* **547** (1992) 473.
[10] A. Trzcińska, J. Jastrzebski, P. Lubinski, F.J. Hartmann, R. Schmidt, T. von Egidy, and B. Klos, *Phys. Rev. Lett.* **87** (2001) 082501.
[11] E. Friedman, *Nucl. Phys. A* **896** (2012) 46; and references therein.
[12] S. Abrahamyan, Z. Ahmed, H. Albataineh, K. Aniol, D.S. Armstrong, W. Armstrong *et al.* (PREX Collaboration), *Phys. Rev. Lett.* **108** (2012) 112502.
[13] B.A. Brown, *Phys. Rev. Lett.* **119** (2017) 122502.
[14] Junjie Yang and J. Piekarewicz, *Phys. Rev. C* **97** (2018) 014314.
[15] B.P. Abbott *et al.* [LIGO Scientific and Virgo Collaborations], *Phys. Rev. Lett.* **119** (2017) 161101.
[16] Eemeli Annala, Tyler Gorda, Aleksi Kurkela, and Aleksi Vuorinen, arXiv:1711.02644 [astro-ph.HE]; and references therein.
[17] J.S. Read *et al.*, *Phys. Rev. D* **79** (2009) 124032.
[18] M. Hoferichter *et al.*, *Phys. Rev. Lett.* **115** (2015) 192301; *Phys. Rep.* **625** (2016) 1.
[19] H. Krebs, A. Gasparyan, and E. Epelbaum, *Phys. Rev. C* **85** (2012) 054006.
[20] J. Antoniadis *et al.*, *Science* **340** (2013) 6131.
[21] J.M. Lattimer and M. Prakash, *Ap. J.* **550** (2001) 426.
[22] A.W. Steiner, J.M. Lattimer, and E.F. Brown, *Astrophys. J.* **765** (2013) L5.